Corrosion Resistance of Dissimilar GTA Welds for Offshore Applications

This work studies the effect of filler metal selection on the corrosion resistance of super duplex/pipeline steel welds

BY W. N. KHAN, R. CHHIBBER, N. SAINI, Y. WANG, R. KOPPARTHI, S. D. CHOUDHURY, AND L. LI

Abstract

The pitting corrosion resistance of dissimilar pipeline steel API X70 and Super Duplex 2507 Stainless Steel gas tungsten arc (GTA) welds was studied. The GTA welds were fabricated using Super Duplex 2594 Filler Metal or austenitic 309L Filler Metal. The specimens extracted from the base metal, weld fusion zone, fusion boundary, and heat-affected zones (HAZs) were subjected to a potentiodynamic corrosion test in a 3.5% NaCl water solution. The weld made using the 309L Filler Metal was found to have a smaller pitting resistance equivalent number (PREN) difference between ferrite and austenite, making it more corrosion resistant than the weld fabricated using the 2594 Filler Metal. The HAZ on the X70 side was the most susceptible to pitting and galvanic corrosion for both filler metals.

Keywords

- Gas Tungsten Arc (GTA) Weld
- Super Duplex 2507
- API X70
- Dissimilar Joints
- Microstructure
- Corrosion

Introduction

API-grade pipeline steels with high strength and toughness are widely used for oil-gas transportation applications in the energy industry (Ref. 1). Drilling risers and transportation pipelines made of API-grade steels may leak, producing environmental damage, due to corrosion and/or stress corrosion. Frequently, the pipeline steel needs to be joined with high-corrosion-resistant alloys to enhance the structural integrity in critical locations (Ref. 2). Super duplex stainless steels, due to their balanced austenite/ferrite ratio, offer a combination of excellent mechanical properties and superior corrosion resistance (Ref. 3). Dissimilar joining of super duplex steel and pipeline steel in critical locations, such as marine splash zones and branching points of the distribution network, is preferred over the sleeve connection because continuous maintenance is required to provide cathodic protection to the sleeves (Ref. 4).

Gas tungsten arc welding (GTAW) is often used for joining dissimilar super duplex and pipeline steels. The filler metal plays an influential role in the microstructure and behavior of dissimilar welds (Ref. 5). Several issues that may lead to potential galvanic corrosion of the dissimilar joints include the difference in carbon concentration, the coefficient of thermal expansion, and phase transformations near the interface causing physical and metallurgical heterogeneities (Ref. 6). Fusion welding methods used to fabricate super duplex steel welds may alter the ferrite to austenite ratio, morphology, and distribution of microstructure zones of the weld joint (Ref. 7).

Super Duplex Stainless Steel Filler Metal ER2594 and austenitic Stainless Steel Filler Metal ER309L are the commonly used filler metals for fabricating super duplex stainless steel/pipeline steel welds (Ref. 8). The difference in the chemical compositions of these filler metals leads to varied microstructure evolution and weld performance (Ref. 9). Repeated
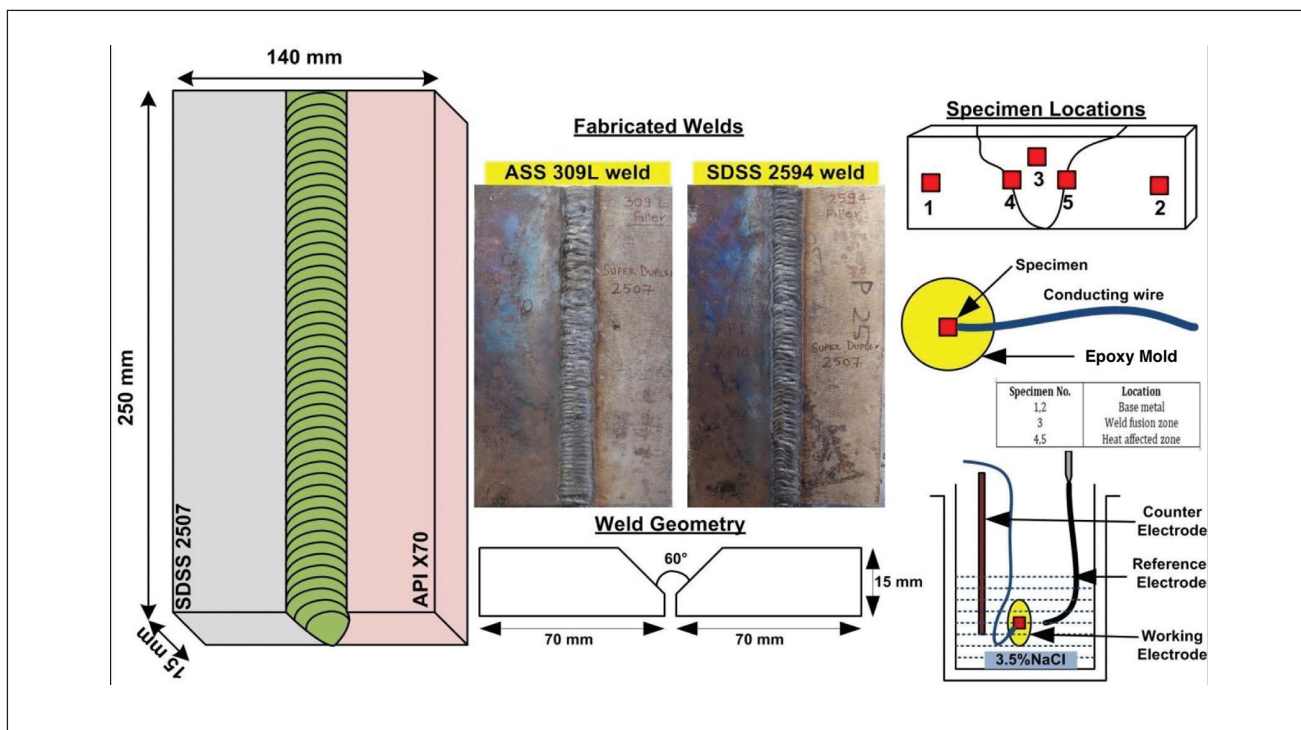
Fig. 1 — Schematic of weld geometry and corrosion investigation.

Table 1 — Measured Chemical Composition of Test Materials (wt-%)

Type	Material	Cr	Ni	Mo	Si	C	Fe	Mn
Base metals	Super Duplex 2507	26.2	6.7	3.6	0.38	0.03	61.10	0.72
	API X70	0.37	0.3	0.001	0.32	0.06	97.50	1.64
Filler metals	ER309L	23.2	13.4	0.1	0.40	0.02	60.80	1.80
	ER2594	25.3	9.6	3.8	0.34	0.01	59.47	0.53

heating and cooling in multipass GTAW sometimes lead to a precipitation of unwanted secondary precipitates in the weld and heat-affected zone (HAZ). The most common precipitates, Cr_2N and secondary austenite, may lead to increased intergranular corrosion in multipass duplex welds (Ref. 10). The addition of N_2 in the shielding gas makes up for the loss of nitrogen, increasing the corrosion resistance of duplex stainless steel welds (Refs. 11, 12). A large heat input leads to excessive formation of ferrite in the HAZ in the duplex stainless steel and subsequent precipitation of deleterious sigma, chi, and carbide phases, particularly during long-term service (Ref. 13). The corrosion resistance of submerged arc welded Duplex 2205 Steel welds depends significantly on the chromium/nickel ratio of the filler wire, ferrite/austenite ratio, elemental diffusion, and groove design (Ref. 14). A higher Cr and Ni concentration in the filler metal compared to the base
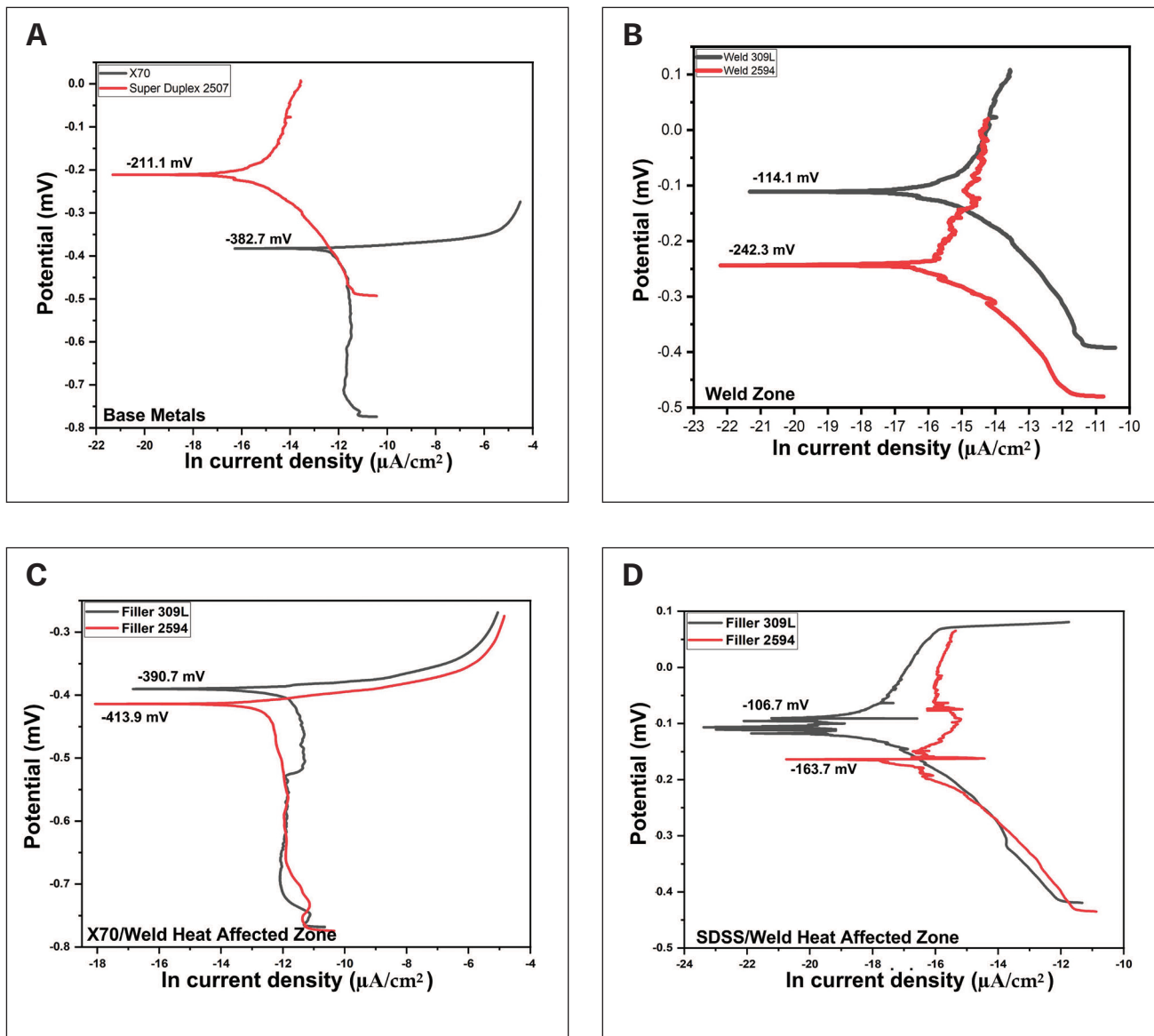
Fig. 2 — Potential vs. logarithm current density plots for different zones of the dissimilar welds: A — Base metals; B — weld fusion zones; C — HAZ on the X70 side; D — HAZ on the super duplex side.

metal helps improve the corrosion resistance of the weld joint (Ref. 15). Experimental investigations indicate the corrosion resistance of the E309L electrode to be superior to E2209's for a dissimilar low-alloy steel/duplex weld fabricated using the shielded metal arc welding (SMAW) process (Ref. 16).

Researchers have studied the dissimilar welding of pipeline steel with high-corrosion-resistant alloys and focused upon texture, mechanical, and metallurgical behavior (Refs. 17, 18). However, not enough information about the role of filler metals on weld formation and the corrosion behavior of dissimilar super duplex/pipeline steel welds is available. Moreover, there seems to be a void in literature correlating filler metals to element partitioning and corrosion resistance of dissimilar welds. When selecting among competing filler metals, austenitic type vs. duplex type, the engineer is not fully aware of the consequences of their choice on weld pitting corrosion resistance.

This work aims to establish the effect of filler metal selection on the corrosion resistance of dissimilar super duplex/ pipeline steel GTA welds. The corrosion resistance of dissimilar welds was compared for the individual weld zones of two different filler metals with direct relevance to galvanic corrosion in welded offshore structures. The results and discussion presented can be applied to the offshore sector with special emphasis on structures employed in aggressive corrosive environments.

Experimental Procedures

API X70 and SDSS2507 base metals were procured in dimensions of 290 × 290 × 15 mm. Two filler metal wires, ER309L and ER2594 (2.4 mm diameter), were used to

Table 2 — Average Chemical Composition (wt-%) Measurements by EDS of the Weld Fusion Zones of 309L and 2594 Filler Metals

	309L Austenite	309L Ferrite	2594 Austenite	2594 Ferrite
Cr	22.73	26.51	25.66	25.96
Fe	60.59	60.94	60.42	60.12
Ni	13.82	9.88	8.78	8.60
Mn	1.77	1.60	0.77	0.70
Si	0.45	0.45	0.42	0.49
Mo	0.55	0.50	3.47	3.81
N	0.11	0.23	0.47	0.32
PREN*	24.46	28.15	43.87	38.53

* For calculating the pitting resistance equivalent of austenite (γ), $PREN_\gamma = [Cr] + 3.3[Mo] + 16[N] - [Mn]$ is used. Since EDS measurements of N are semiquantitative, this calculation is only valid for relative ranking. For both high-temperature (δ) and low-temperature (α) ferrite, $PREN_\delta = PREN_\alpha = [Cr] + 3.3[Mo]$ is used (Ref. 20).

fabricate the weld joints. Table 1 lists the chemical composition of these test alloys.

Weld coupons with dimensions of 250 × 70 × 15 mm were extracted from the base metal plates. The edges of the coupons were machined to an angle of 30 deg to obtain a single-V-groove joint design of 60 deg. The coupons were cleaned with acetone to remove dirt, oil, oxide scales, and other contaminants present on the surface. A constant current GTAW with a 2.4-mm AWS-EWTH-2 (98% W + 2% Th) tungsten electrode was conducted in the direct current electrode negative mode. The average heat input was maintained at 0.51 kJ/mm at a constant current of 170 A while the cold wire was fed at a rate of 8 cm/min. The electrode tip-to-work distance was maintained at 3 mm, and the welding speed was kept at 3 mm/s. Pure argon gas (99.9%) at a flow rate of 15 L/min was supplied to shield the molten weld pool. No preheat or postweld heat was used for the 11 passes to fill the V groove.

Quantitative assessment of the corrosion was conducted by electrochemical methods for open circuit potential (OCP) and Tafel analysis. A potentiostat with three-electrode cells was used to measure the specimen's corrosion characteristics in a 3.5% NaCl water solution at a scan rate of 0.167 mV/s in the potential range of ± 0.25 V against the OCP. The OCP was obtained by leaving the specimen in the electrolytic solution for 6000 s. The potentiostat used an Ag/AgCl electrode, a graphite rod, and the specimen under investigation as the reference, counter, and work electrode, respectively. The
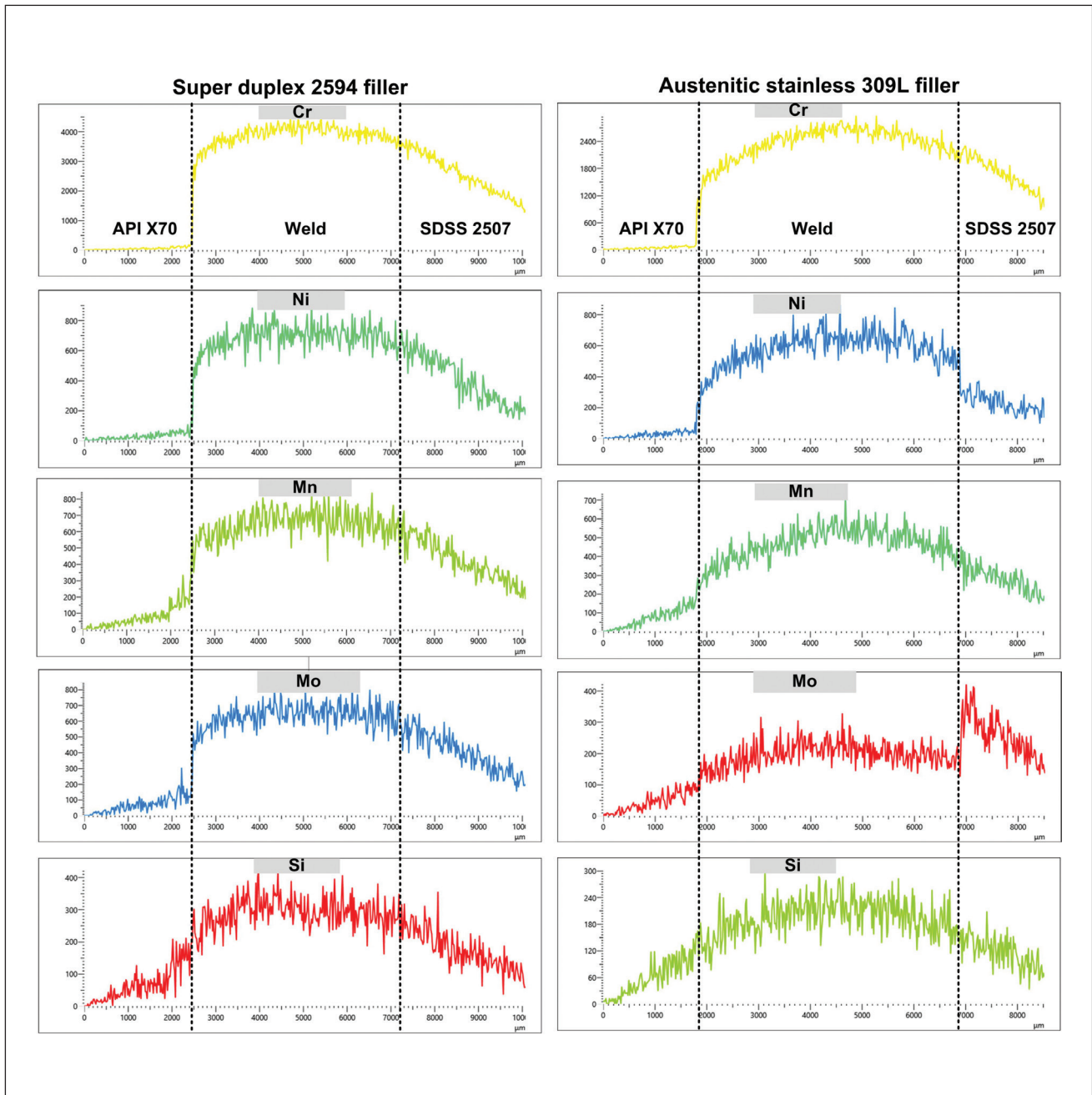
Fig. 3 — EDS line scans of alloying elements across the weld and HAZs. The Y-axis is intensity (arbitrary unit), and the X-axis is distance in micrometers. The dashed lines indicate the locations of the fusion boundaries.

investigated specimens were 2 × 2 × 15 mm extracted from the base metal, weld fusion zone, fusion line, and HAZ on both sides of the weld, as shown in Fig. 1. The weld joint was etched to reveal microstructure regions before extracting the corrosion specimens so that each specimen only contained material from one specific weld region. Before being exposed to the aqueous environment, the test specimens were mounted in epoxy, and the surface was cleaned by grinding through successive grits from size #80 to #600. The specimen surface was further cleaned with acetone to remove any contamination.

Results

In the Tafel analysis, a potential scan of ± 25 mV around the open circuit voltage is imposed on the metal specimen, and the current is recorded. A linear relationship exists between the current and voltage in this voltage range, and the slope is the polarization resistance (R_p), which is the resistance of the metal to oxidation under the external potential. The corrosion current (I_{corr}) is inversely related to R_p, as shown in Equation 1 (Ref. 19):
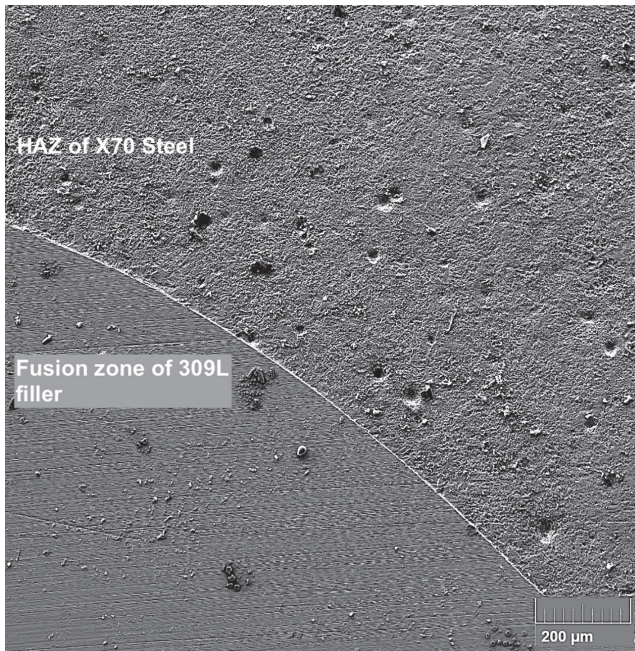
Fig. 4 — As-corrosion-tested surface of the fusion line with X70 Steel. The 309L Filler Metal fusion zone is pitting free (the particles are adhered corrosion products), while the HAZ of X70 steel is pitted.

$$I_{corr} = \frac{\beta_a \beta_c}{2.3 R_p (\beta_a + \beta_c)} \qquad (1)$$

where β_a is the anodic Tafel slope, and β_c is the cathodic Tafel slope. A higher corrosion current I_{corr} indicates a higher corrosion rate.

Figure 2 shows the Tafel curves of all test specimens in 3.5% NaCl solution. The corrosion current I_{corr} of the X70 pipeline base metal was found to be 83.62 nA, which was significantly higher than the 547.6 pA of the Super Duplex 2507 base metal. For the weld fusion zone specimens, the I_{corr} of E309L Filler Metal was 44.65 pA, which was much lower than 227 pA for the Super Duplex 2594 Filler Metal. For the X70 HAZ specimens, the I_{corr} for the 309L Filler Metal and Super Duplex 2594 Filler Metal was 48.03 and 41.16 nA, respectively. For the Super Duplex 2507 HAZ specimens, the I_{corr} for the 309L Filler Metal and Super Duplex 2594 Filler Metal was 69.26 and 97.1 pA, respectively. The corrosion current is thus ranked from high to low, the higher being less corrosion resistant: X70 base metal > X70 HAZ > 2507 base metal > 2594 Filler Metal > 2507 HAZ > 309L Filler Metal.

For high-corrosion-resistant alloys (both austenitic and duplex stainless), the repassivation would be fast. It may have given rise to the nonlinearity in the Tafel curves for stainless steels in Fig. 2, introducing some errors in identifying the β_a and β_c slopes. Besides, the HAZ specimens do contain a
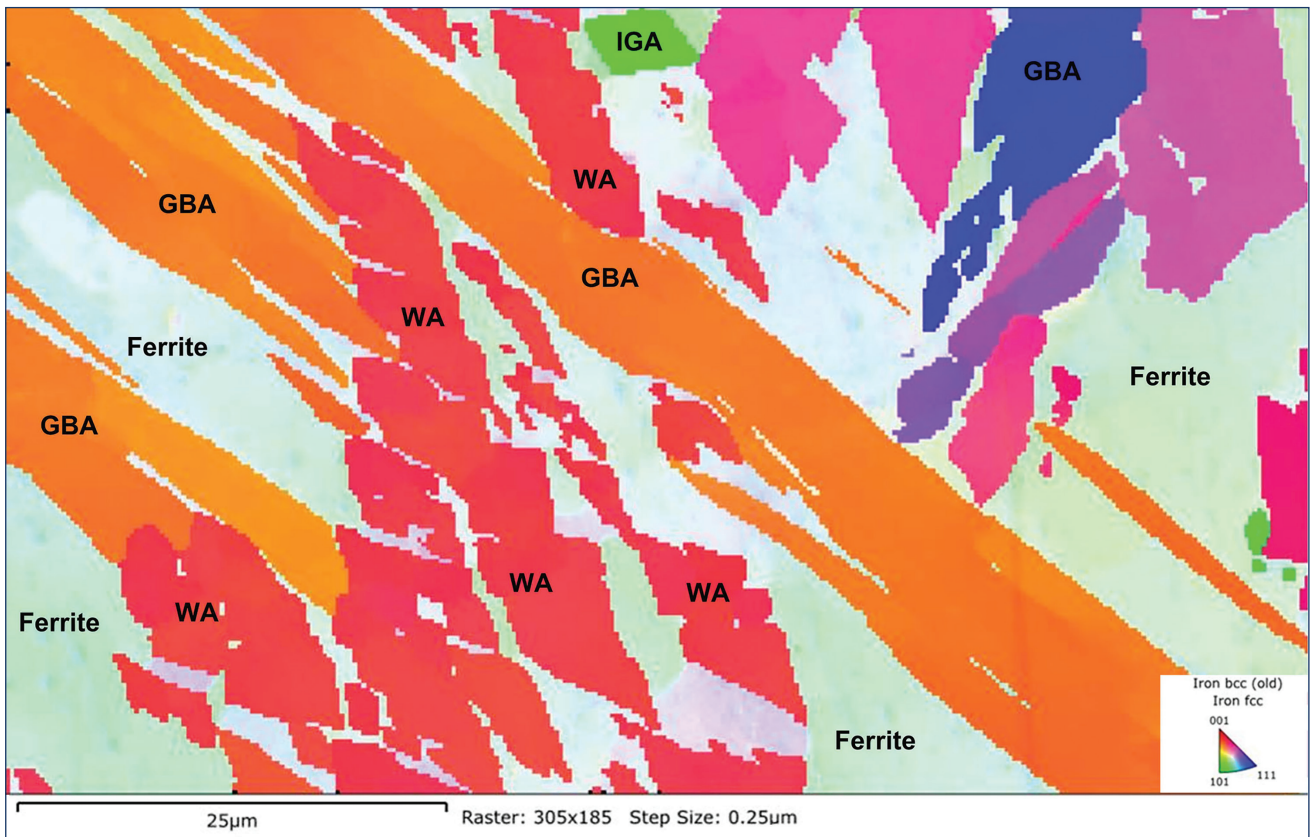
Fig. 5 — EBSD phase map of the weld made by the Super Duplex 2594 Filler Metal.
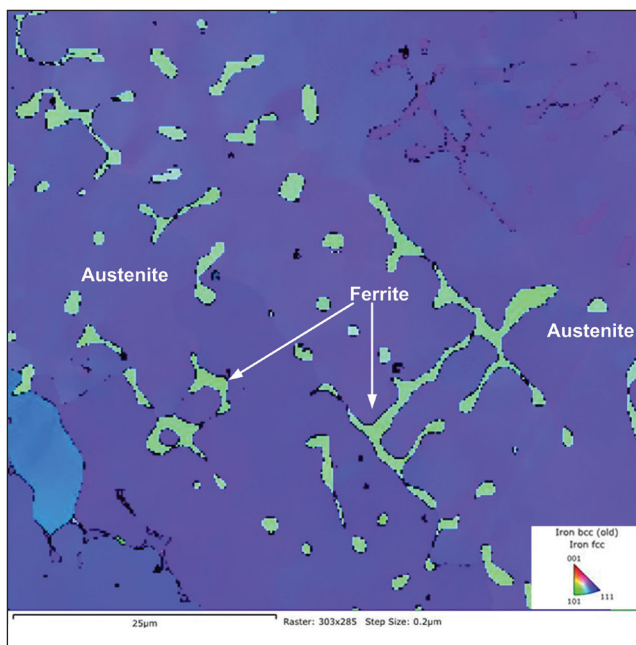
Fig. 6 — EBSD phase map of the weld made by the austenitic 309L Filler Metal.

small amount of fusion boundary material, which would have decreased the corrosion current estimation.

The corrosion potential (E_{corr}), therefore, is a more reliable measurement for corrosion resistance. From Fig. 2A, the E_{corr} of API X70 base metal (–382.7 mV) was lower compared to that of Super Duplex Stainless Steel 2507 (–211.1 mV). From Fig. 2B, the E_{corr} of the weld made with 309L Filler Metal (–114.1 mV) was found to be superior to the weld made with Super Duplex 2594 Filler Metal (–242.3 mV). Shown in Fig. 2C, the E_{corr} for the fusion line and HAZ on the X70 side for both filler metals was low: –390.7 mV for the 309L Filler Metal and –413.9 mV for the 2594 Filler Metal, respectively. The HAZ on the X70 side was clearly the weakest link for corrosion resistance across the weld joints. The E_{corr} for the fusion line and HAZ on the Super Duplex 2507 side for both filler metals was nobler: –106.7 mV for the 309L Filler Metal and –163.7 mV for the 2594 Filler Metal, respectively (Fig. 2D). The corrosion resistance of the super duplex HAZ was better than that of the base metal Super Duplex 2507. Ranking by E_{corr} from the least noble for corrosion is as follows: X70 HAZ > X70 base metal > 2594 Filler Metal > 2507 base metal > 2507 HAZ > 309L Filler Metal. This E_{corr} ranking agrees in trend with the I_{corr} ranking, although it identifies the X70 HAZ as the least corrosion-resistant region of the weld joints.

The energy dispersive spectroscopy (EDS) line scans across the two weld joints are shown in Fig. 3. In the super duplex filler weld fusion zone, all elements were at a higher level than either of the base metals. The same is true for the austenitic filler weld fusion zone, except Mo, which had a higher level in the duplex base metal. There was a sharp drop of Cr and Ni and a more gradual slope of Mn, Mo, and Si across the fusion line on the X70 side of the HAZs. On the super duplex side, all elements showed a gradual slope across the fusion boundaries — Fig. 3.

The scanning electron microscopy images of corroded specimens revealed the pitting to be concentrated in the X70 HAZ. Shown in Fig. 4 is an example micrograph for the 309L Filler Metal weld, confirming the lowest ranking of X70 HAZ by E_{corr} for corrosion resistance.

Discussion

Past research suggested that the overall resistance to pitting corrosion of a duplex microstructure can be determined by the pitting susceptibility of the less-resistant phase (Refs. 21–23). The difference between the pitting resistance equivalent number (PREN) of the two phases can be used to predict pitting resistance. A smaller difference in the PREN values between ferrite (γ) and austenite (γ), $\Delta = (PREN_\alpha - PREN_\gamma)$, predicts a possibly higher pitting corrosion resistance.

Figure 5 shows the electron backscatter diffraction (EBSD) phase map of the weld fusion zone made with the Duplex Stainless Steel 2594 Filler Metal. Figure 6 shows the EBSD phase map of the weld fusion zone made with the austenitic 309L Filler Metal. Clearly, both welds consisted of a ferrite and austenite duplex microstructure. The primary solidification mode of both the filler metals is the same; however, upon subsequent cooling, the chemical composition differed significantly. Due to the difference in chemical composition of the two filler metals, the segregation of alloying elements, particularly Cr and Mo, also varied for both welds. Hence, the resultant PREN for the austenite and ferrite phases in the two welds differed. The back-scattered electron beam images and EDS measurements for the chemical composition of the specimens are listed in Table 2. It is notable that the 309L Filler Metal weld has a ($PREN_\alpha - PREN_\gamma$) difference of |24.46 – 28.15| = 3.69 while the 2594 Filler Metal weld has a ($PREN_\alpha - PREN_\gamma$) difference of |38.52 – 43.87| = 5.35. The smaller difference for the 309L Filler Metal weld predicts a greater pitting corrosion resistance than the 2594 Filler Metal weld (Ref. 24).

The thermodynamic reason for the chemical segregation shown in Table 2 is explained next. Scheil solidification calculations consider an intermediate cooling rate, under which a complete mixing in the liquid and no solid-state diffusion are consequently assumed. For the 309L Filler Metal weld, molten pool solidification started at 1443°C and finished at 1291°C. Element partitioning between ferrite and austenite during the solidification is shown in Fig. 7 for the weld made from the 309L Filler Metal. Predicted enrichment of Cr and Mo in the ferrite phase was shown to agree with the EDS measurements in Table 2.

For the weld made with the 2594 Filler Metal, molten pool solidification started at 1492°C and finished at 1406°C. Element partitioning between ferrite and austenite during the solidification is shown in Fig. 8 for the 2594 Filler Metal weld. Again, predicted enrichment of Cr and Mo in the ferrite phase was shown to agree with the EDS measurements in Table 2.

Based on this discussion, it is suggested that 309L Filler Metal would be preferred for dissimilar welding, although the results with either of these fillers would be acceptable for service as measured by the Tafel curves. In addition, it must be understood that the corrosion testing was only in
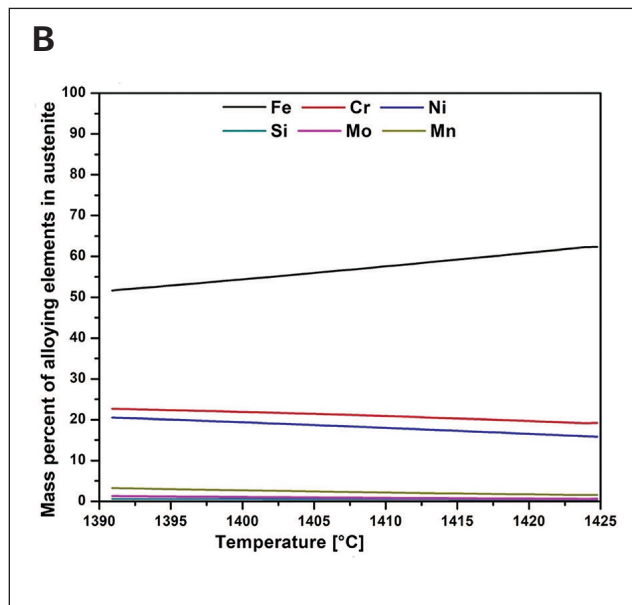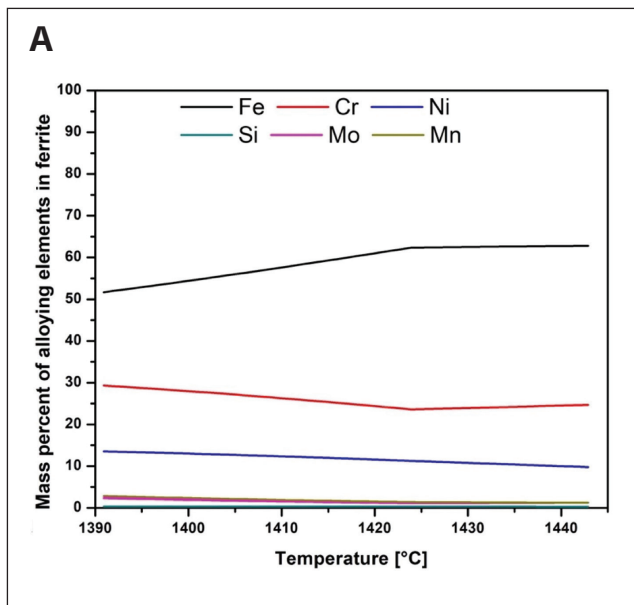
Fig. 7 — Thermo-Calc–predicted chemical composition of δ-ferrite (A) and austenite (B) near the transition temperatures (1425° to 1390°C) of the weld fusion zone made with the 309L Filler Metal.
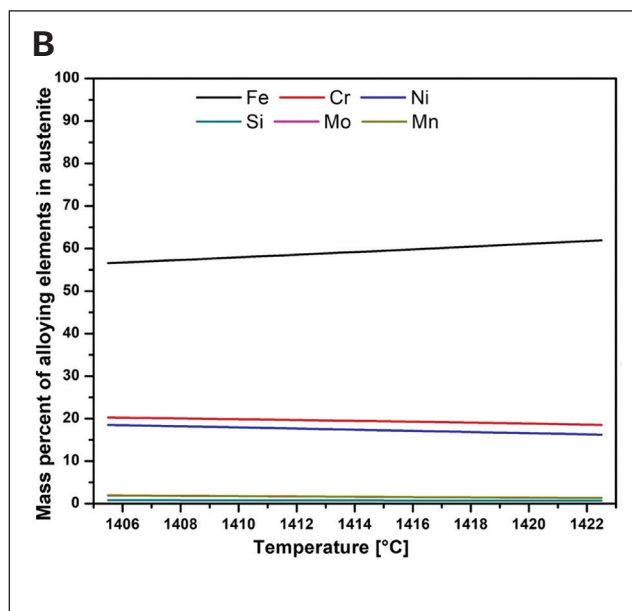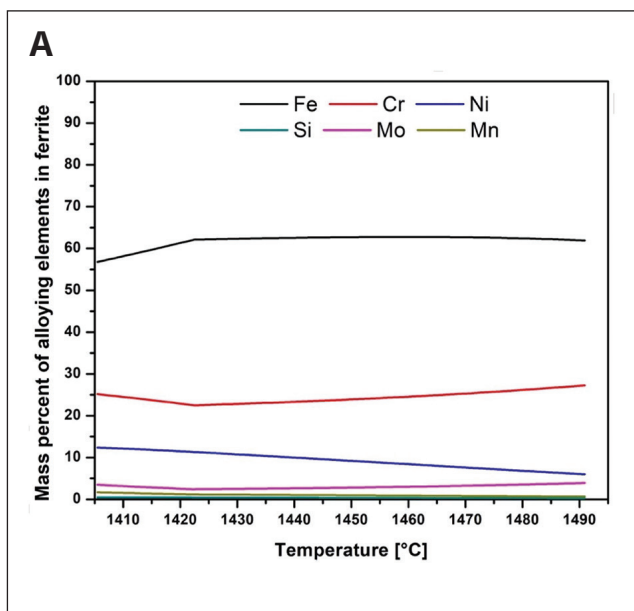
Fig. 8 — Thermo-Calc–predicted chemical composition of δ-ferrite (A) and austenite (B) near the transition temperatures (1490° to 1400°C) of the weld fusion zone made with the 2594 Filler Metal.

one environment (3.5% NaCl water solution). In other environments, welds made with Super Duplex 2594 Filler Metal may have better performance.

The reason the HAZ of X70 was the weakest link for corrosion resistance is suggested due to primarily a galvanic coupling with a high-alloyed weld fusion zone and secondarily due to a loss of dissolved Cr and the formation of high-angle grain boundaries. The HAZ on the X70 side is susceptible to second-phase precipitations, which are usually shown as martensite-austenite (M/A) constituents and carbides in the proximity of the fusion line (Ref. 25). EBSD analysis of the X70 HAZ revealed that, for both filler metals, the grain boundaries in this region had a small amount of precipitation of Cr_7C_3 (Fig. 9), which may lead to a loss of dissolved Cr in the ferrite matrix. However, the HAZ also had a presence of some unindexed pixels due to the instrument's limitations. The grain boundaries in the HAZ of X70 steel were, thus, the most susceptible region for the initiation of pitting due to high-angle grain boundaries and loss of Cr to carbides. The significant difference in the PREN of the two phases and high-angle grain boundaries make the grain boundary the most likely site for pit initiation.
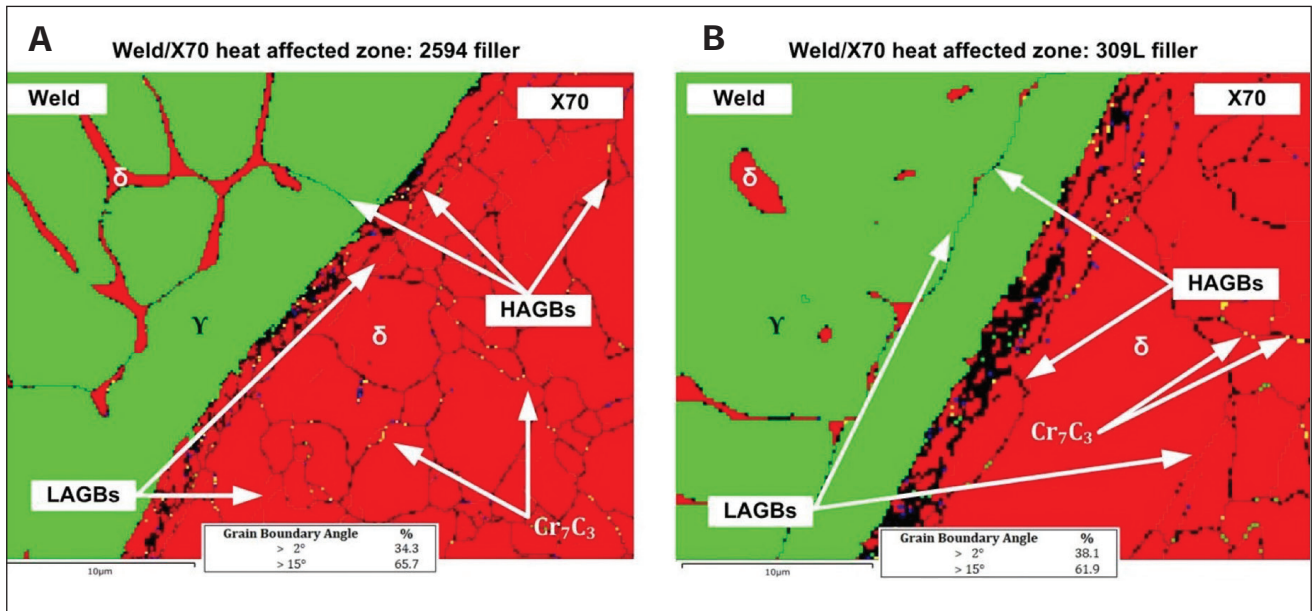
Fig. 9 — Grain boundaries in the HAZ on the X70 Steel side: A — Weld made with 2594 Filler Metal; B — weld made with 309L Filler Metal.
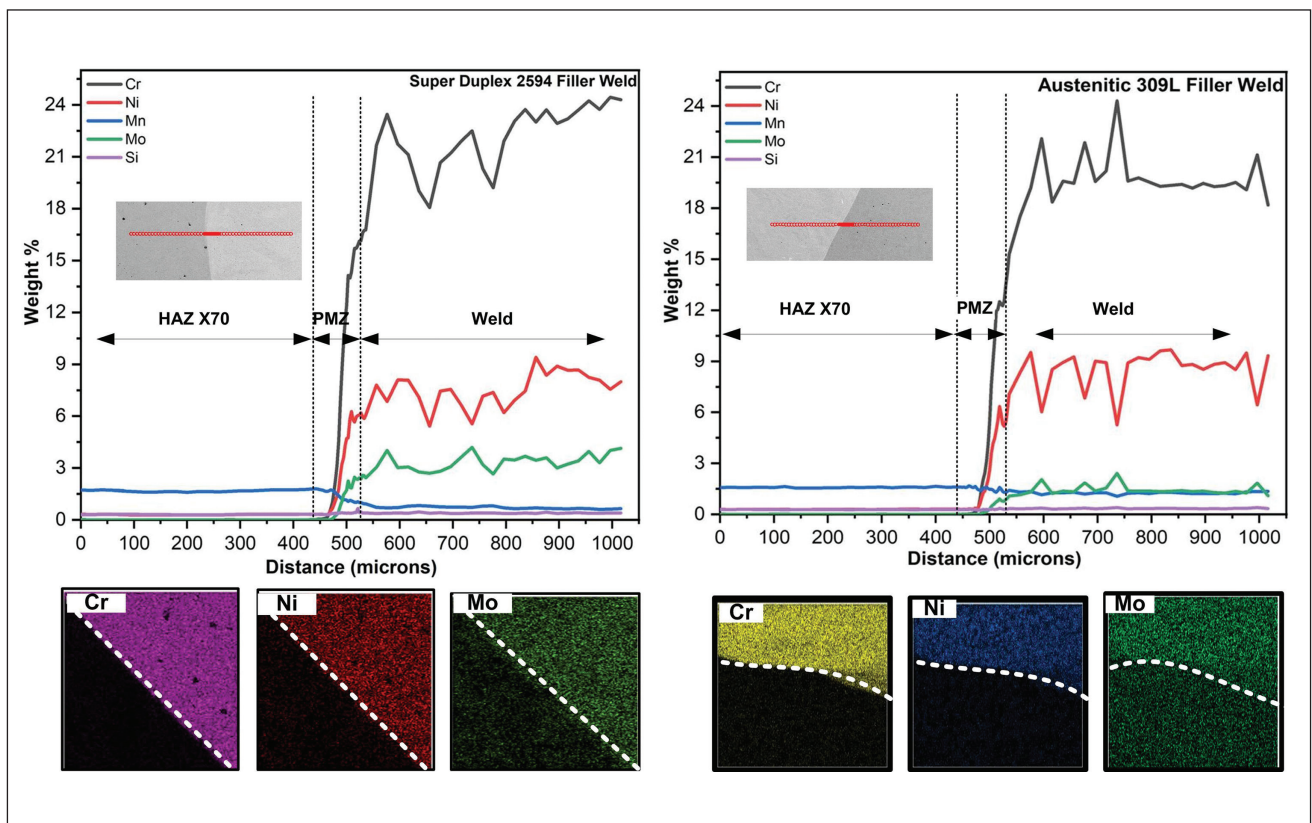
Fig. 10 — Quantitative elemental analysis at X70 HAZ and weld fusion zones by both filler metals.

The elemental composition by electron probe microanalyzer quantitative analysis and corresponding element maps obtained using EDS at the X70/weld interface are presented in Fig. 10. The measurement was taken over a length of approximately 1000 μm, covering the HAZ, fusion line, and weld fusion zone. The elemental composition plots of both the filler metal welds suggest almost negligible presence of Cr, Ni, and Mo in the HAZ region of the X70 Steel. These elemental compositions witnessed a sharp increase in the region of fusion boundary into the weld fusion zone. Such

distribution of Cr suggests the susceptibility of X70 welded to stainless steel to corrode by a simple galvanic mechanism (i.e., both filler metals being much more electropositive than the X70 in the presence of seawater). This chemical composition distribution explains the large negative corrosion potentials for the X70 HAZ in Fig. 2C.

Conclusions

The pitting corrosion resistance of the weld made with the 309L Filler Metal is superior compared to that of the Super Duplex 2594 weld due to a smaller difference in the PREN between ferrite and austenite. The HAZ on the X70 side is the region most susceptible to pitting initiation in the entire weld joint. The general corrosion of the HAZ on the X70 side may be driven by a galvanic couple (i.e., both filler metals being more electropositive than the X70 in the presence of seawater).

It is suggested that 309L Filler Metal would be preferred for the dissimilar welding of API X70 and Super Duplex 2507, although the results of either 309L or 2594 Filler Metals would be acceptable for corrosion service in salt water. In addition, it must be understood that the corrosion testing in this study was only in one environment (3.5% NaCl solution). In other environments, welds made with Super Duplex 2594 Filler Metal may have better performance.

References

1. Kannan, R., Li, L., Guo, L., Anderson, N., Rashid, M., Collins, L., and Arafin, M. 2020. Bond formation mechanism for resistance welding of X70 pipeline steel. *Welding Journal* 99(8): 209-s to 223-s. DOI: 10.29391/2020.99.020

2. Khan, W. N., and Chhibber, R. 2020. Weld metal chemistry of mineral waste added SiO_2-CaO-CaF_2-TiO_2 electrode coatings for offshore welds. *Journal of Pressure Vessel Technology* 142(3): 031505. DOI: 10.1115/1.4046218

3. Magalhaes, A. S., Magalhaes, C. H. X. M., De Lima, M. S. F., Cruz, J., Godefroid, L. B., Bertazzoli, R., and De Faria, G. L. 2020. Effect of PWHT on laser-welded duplex stainless steel. *Welding Journal* 99(7): 185-s to 202-s. DOI: 10.29391/2020.99.018

4. Mendoza, B. I., Maldonado, Z. C., Albiter, H. A., and Robles, P. E. 2010. Dissimilar welding of super duplex stainless steel/HSLA steel for offshore applications joined by GTAW. *Engineering* 2(7): 520–528. DOI: 10.4236/engineering.2010.27069

5. Saini, N., Mulik, R. S., and Mahapatra, M. M. 2019. Influence of filler metals and PWHT regime on the microstructure and mechanical property relationships of CSEF steel dissimilar welded joints. *International Journal of Pressure Vessels and Piping* 170: 1–9. DOI: 10.1016/j.ijpvp.2019.01.005

6. Chhibber, R., Arora, N., Gupta, S. R., and Dutta, B. K. 2006. Use of bimetallic welds in nuclear reactors: Associated problems and structural integrity assessment issues. *Proceedings of the Institution of Mechanical Engineers, Part C: Journal of Mechanical Engineering Science* 220(8): 1121–1133. DOI: 10.1243/09544062JMES135

7. Meinhardt, C. P., Scheid, A., Santos, J. F., Bergmann, L. A., Favaro, M. V., and Kwietniewski, C. E. F. 2017. Hydrogen embrittlement under cathodic protection of friction stir welded UNS S32760 super duplex stainless steel. *Materials Science & Engineering: A* 706: 48–56. DOI: 10.1016/j.msea.2017.08.117

8. Khan, W. N., and Chhibber, R. 2021. Experimental investigation on dissimilar weld between super duplex stainless steel 2507 and API X70 pipeline steel. *Proceedings of the Institution of Mechanical Engineers, Part L: Journal of Materials: Design and Applications* 235(8): 1827–1840. DOI: 10.1177/14644207211013056

9. Sun, K., Zeng, M., Shi, Y., Hu, Y., and Shen, X. 2018. Microstructure and corrosion behavior of S32101 stainless steel underwater dry and wet welded joints. *Journal of Materials Processing Technology* 256: 190–201. DOI: 10.1016/j.jmatprotec.2018.02.018

10. Zhang, Y., Cheng, S., Wu, S., and Cheng, F. 2020. The evolution of microstructure and intergranular corrosion resistance of duplex stainless steel joint in multi-pass welding. *Journal of Materials Processing Technology* 277: 116471. DOI: 10.1016/j.jmatprotec.2019.116471

11. Lai, R., Cai, Y., Wu, Y., Li, F., and Hua, X. 2016. Influence of absorbed nitrogen on microstructure and corrosion resistance of 2205 duplex stainless steel joint processed by fiber laser welding. *Journal of Materials Processing Technology* 231: 397–405. DOI: 10.1016/j.jmatprotec.2016.01.016

12. Jegdic, B., Bobic, B., Radojkovic, B., Alic, B., and Radovanovic, L. 2019. Corrosion resistance of welded joints of X5CrNi18-10 stainless steel. *Journal of Materials Processing Technology* 216: 579–587. DOI: 10.1016/j.jmatprotec.2018.11.029

13. Shi, Y., Cui, S., Zhu, T., Gu, S., and Shen, X. 2018. Microstructure and intergranular corrosion behavior of HAZ in DP-TIG welded DSS joints. *Journal of Materials Processing Technology* 256: 254–261. DOI: 10.1016/j.jmatprotec.2018.02.019

14. Wu, M., Liu, F., Pu, J., Anderson, N. E., Li, L., and Liu, D. 2017. The microstructure and pitting resistance of weld joints of 2205 duplex stainless steel. *Journal of Materials Engineering and Performance* 26: 5341–5347. DOI: 10.1007/s11665-017-2976-0

15. Davis, J. R., ed. 2006. *Corrosion of Weldments*, 43–75. Materials Park, Ohio: ASM International.

16. Srinivasan, P. B., Muthupandi, V., Dietzel, W., and Sivan, V. 2006. Microstructure and corrosion behavior of shielded metal arc-welded dissimilar joints comprising duplex stainless steel and low alloy steel. *Journal of Materials Engineering and Performance* 15: 758–764. DOI: 10.1361/105994906X150902

17. Eghlimi, A., Shamanian, M., Eskandarian, M., Zabolian, A., and Szpunar, J. A. 2015. Characterization of microstructure and texture across dissimilar super duplex/austenitic stainless steel weldment joint by super duplex filler metal. *Materials Characterization* 106: 27–35. DOI: 10.1016/j.matchar.2015.05.017

18. Khan, W. N., and Chhibber, R. 2021. Effect of filler metal on solidification, microstructure and mechanical properties of dissimilar super duplex/pipeline steel GTA weld. *Materials Science and Engineering: A* 803: 140476. DOI: 10.1016/j.msea.2020.140476

19. Zaveri, N., Mahapatra, M., Deceuster, A., Peng, Y., Li, L., and Zhou, A. 2008. Corrosion resistance of pulsed laser-treated Ti-6Al-4V implant in simulated biofluids. *Electrochimica Acta* 53(15): 5022–5032. DOI: 10.1016/j.electacta.2008.01.086

20. Bailey, S. I., and Li, X. 2012. Corrosion of stainless steels in the marine splash zone. *Advanced Materials Research* 610–613: 272–275. DOI: 10.4028/www.scientific.net/AMR.610-613.272

21. Amiri, E., Ostovan, F., Toozandehjani, M., Shafiei, E., and Mohamed, I. F. 2021. Study and selection of most appropriate filler rod for GTAW of S32750 super duplex steel joints: A comprehensive study on microstructural mechanical and corrosion properties. *Materials Chemistry and Physics* 270: 124839. DOI: 10.1016/j.matchemphys.2021.124839

22. Ha, H.-Y., Jang, M.-H., Lee, T.-H., and Moon, J. 2014. Interpretation of the relation between ferrite fraction and pitting corrosion resistance of commercial 2205 duplex stainless steel. *Corrosion Science* 89: 154–162. DOI: 10.1016/j.corsci.2014.08.021

23. Lee, J.-S., Fushimi, K., Nakanishi, T., Hasegawa, Y., and Park, Y. -S. 2014. Corrosion behaviour of ferrite and austenite phases on super duplex stainless steel in a modified green-death solution. *Corrosion Science* 89: 111–117. DOI: 10.1016/j.corsci.2014.08.014

24. Ha, H.-Y., Jang, M.-H., Lee, T.-H., and Moon, J. 2014. Interpretation of the relation between ferrite fraction and pitting corrosion resistance of commercial 2205 duplex stainless steel. *Corrosion Science* 89: 154–162. DOI: 10.1016/j.corsci.2014.08.021

25. Huda, N., Midawi, A. R. H., Gianetto, J., Lazor, R., and Gerlich, A. P. 2016. Influence of martensite-austenite (MA) on impact toughness of X80 line pipe steels. *Materials and Science Engineering: A* 662: 481–491. DOI: 10.1016/j.msea.2016.03.095

WARIS NAWAZ KHAN, NITIN SAINI, YAJING WANG, RAVI-KIRAN KOPPARTHI, SUVAN DEV CHOUDHURY, and **LEIJUN LI** (*leijun@ualberta.ca*) are with the Department of Chemicals and Materials Engineering, University of Alberta, Canada. **RAHUL CHHIBBER** is with the Department of Mechanical Engineering, Indian Institute of Technology Jodhpur, India. **WANG** is also with the College of Materials Science and Engineering, Taiyuan University of Science and Technology, China.

Can We Talk?

The *Welding Journal* staff encourages an exchange of ideas with you, our readers. If you'd like to ask a question, share an idea, or voice an opinion, you can call, write, or email. Staff email addresses are listed below, along with a guide to help you interact with the right person.

Publisher/Editor
Annette Alonso, *aalonso@aws.org, ext.* 299
General Management, Reprint Permission,
Copyright Issues, Editorial Content

Managing Editor
Kristin Campbell, *kcampbell@aws.org, ext.* 257
Feature Articles

Sr. Editor
Cindy Weihl, *cweihl@aws.org, ext.* 256
Section News, *SPRAYTIME®*

Associate Editors
Alexandra Quiñones, *aquinones@aws.org, ext.* 465
Arc-Tist Corner, Industry News
Katie Pacheco, *kpacheco@aws.org, ext.* 275
Society News, New Products

Education Editor
Roline Pascal, *rpascal@aws.org, ext.* 303
Coming Events, Personnel

Managing Editor, Digital and Design; Editor of *Inspection Trends* and *Welding Journal en Español*
Carlos Guzman, *cguzman@aws.org, ext.* 348
Inspection and Spanish-Language Content,
Design and Production

Production Manager
Zaida Chavez, *zaida@aws.org, ext.* 265
Design and Production

Assistant Production Manager
Brenda Flores, *bflores@aws.org, ext.* 330
Design and Production, Peer Review Coordinator

Advertising
Scott Beller, *sbeller@aws.org, ext.* 319
Lea Owen, *lea@aws.org, ext.* 220

Subscriptions
Marandi Gills, *mgills@aws.org, ext.* 353